Structural and magnetic phase transitions in simple oxides using hybrid functionals

M. Alfredsson[a]; J. P. Brodholt[a]; P. B. Wilson[a]; G. D. Price[a]; F. Corà[b]; M. Calleja[c]; R. Bruin[c]; L. J. Blanshard[d]; R. P. Tyer[d]

[a] Department of Earth Sciences, University College London, London, UK [b] Davy Faraday Research Laboratory, The Royal Institution of GB, London, UK [c] Department of Earth Sciences, Cambridge University, Cambridge, UK [d] Daresbury Laboratory, Warrington, Cheshire, UK

PLEASE SCROLL DOWN FOR ARTICLE

Structural and magnetic phase transitions in simple oxides using hybrid functionals

M. ALFREDSSON**, J. P. BRODHOLT*, P. B. WILSON*, G. D. PRICE*, F. CORÀ†, M. CALLEJA‡, R. BRUIN‡, L. J. BLANSHARD§ and R. P. TYER§

*Department of Earth Sciences, University College London, Gower Street, London WC1E 6BT, UK
†Davy Faraday Research Laboratory, The Royal Institution of GB, 21 Albemarle Street, London W1C 4SE, UK
‡Department of Earth Sciences, Cambridge University, Downing Street, Cambridge CB2 3EQ, UK
§Daresbury Laboratory, Daresbury, Warrington WA4 4AD, Cheshire, UK

We present the structural as well as elastic properties of the alkaline earth oxides and FeO, calculated using hybrid exchange functionals within DFT. We show that by empirically fitting the amount of Fock-exchange in the hybrid functionals, we can accurately reproduce the pressure-induced phase transitions for MgO, CaO, SrO and BaO. For FeO the hybrid functionals predict an insulator $\leftrightarrow$ metal transition at ca. 150 GPa, associated with an i-B8 $\leftrightarrow$ B8 structural phase transition. The structural phase transition is accompanied by a spin transition from a high- to low-spin electron configuration on the Fe^{2+} ions. Hence, FeO undergoes a magnetic phase transition from an anti-ferromagnetic to non-magnetic structure. We also find that as the ionicity of the polymorphs increases a higher fraction of Fock-exchange is required to reproduce the structural volumes reported from experiments.

Keywords: Alkaline earth oxide; FeO; DFT; GGA; LDA; Hybrid functional

1. Introduction

Despite its popularity among mineral physicists density functional theory (DFT) suffers from well-known short-comings [1]:

1. The local density approximation (LDA) often underestimates experimentally reported volumes, while the generalised gradient approximation (GGA) functionals (e.g. PW91 and BLYP) overestimate the volumes (see for example Refs. [1–3]).
2. Because the values of calculated bulk moduli depend on the inverse equilibrium volumes, the LDA overestimates and the GGA techniques underestimate the experimentally reported values of bulk moduli [2,3].
3. LDA often underestimates, while GGA overestimates experimentally observed pressures of phase transitions [1,3,4].
4. DFT often fails in reproducing systems containing highly localised *d*- and *f*-electrons [1], including Fe containing minerals, such as Fe-silicates and oxides, wrongly predicting these minerals being metals, while they are in fact insulators.

Our approach to improve on the DFT accuracy is to use so called hybrid DFT exchange functionals. These are obtained by empirically mixing the DFT exchange with different amounts of Hartree-Fock (HF) exchange. The mixing coefficient can be treated as an empirical parameter, and chosen in such a way that calculated properties best reproduce available experimental observations. The best known hybrid DFT functional is Becke's 3-parameter exchange often used in combination with the Lee-Yang-Parr (LYP) correlation functional (B3LYP) [5,6]. In a previous study, we have reported the success of hybrid functionals in modelling the B1 structure of FeO (wüstite) [7]. The hybrid functionals have also been successful in reproducing structural, electronic and magnetic properties of similar compounds, for example NiO [8–10], VO [11] and $BaTiO_3$ [12], and the performance of hybrid functionals in the solid state was recently reviewed by Corà *et al.* [13], including work on the related structures MnO and NiO studied by Middlemiss and Mackrodt. We here extend our work on structural and elastic properties, to include the performance of hybrid functionals in describing structural and magnetic phase transitions. Only one study has, to our knowledge, been published using hybrid functionals to study phase transitions [14]. Here we present results for five different oxides, namely: FeO, BaO, SrO, CaO and MgO.

*Corresponding author. E-mail: m.alfredsson@ucl.ac.uk

All five oxides discussed here are stable in the B1 or a rhombohedrally distorted B1 (r-B1) structure at zero temperature and pressure. However, as we increase the pressure they undergo different phase transitions as schematically shown in figure 1. In particular, MgO (periclase), CaO (lime) and SrO show a B1 ↔ B2 phase transition [15–22] (figure 1a) that has been frequently studied in the literature employing different computational techniques (see for example Refs. [3,18–22]). MgO may exist in the lower mantle of the Earth, and, is thus, expected to be one of the most common minerals in the Earth [23]. CaO is an important material used for construction work and in steel manufacturing [24,25]. Lime is also utilised for arsenic removal; as softener in drinking water; and for flue gas treatment [25]. Here, we have chosen to study CaO because it has a well-characterised B1 ↔ B2 phase

transition, reported to occur at around 60 GPa [15,16,19–22,26]. Experimental studies on MgO have only been possible up to ca. 200 GPa, in which range no phase transition is reported [27]. From theoretical studies the phase transition in MgO is predicted to occur at pressures between 450 and 660 GPa [3,18,21,28–30]. For comparison we will also discuss the B1–B2 transition in SrO, which is experimentally [17] and theoretically [3,19–22] reported to occur at around 36 GPa.

BaO has at least two experimentally observed structural phase transitions B1 ↔ i − B8 ↔ PH$_4$I (figure 1b) at 10 and 15 GPa, respectively, and eventually a third transition between the PH$_4$I ↔ B2 structures at pressures above 60 GPa [31,32]. In the B1 structure, both cations and anions are in octrahedrally coordinated sites. In the i-B8 structure the anions remain octrahedrally coordinated,

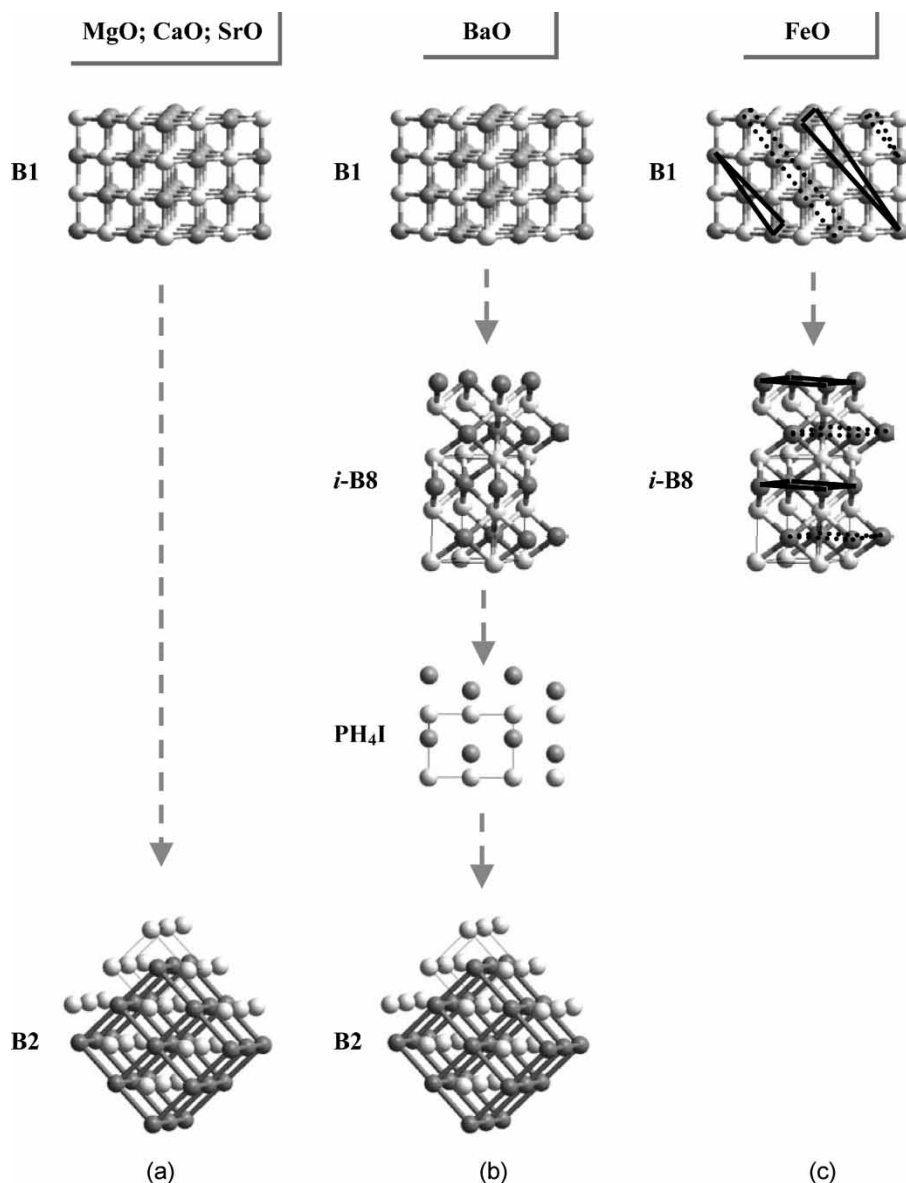Figure 1.   Proposed structural phase transitions for (a) MgO, CaO and SrO, (b) BaO, and (c) FeO. Arrows indicate increasing pressure. Light grey and dark grey balls indicate oxygen ions and cations, respectively. For FeO planes with opposite spins are marked with dotted and full lines. The B8 structure discussed in the text is derived from the i-B8 structure, by changing the atomic positions for the oxygen ions and cations.

while the cations are in a bi-pyramidal site still with six nearest neighbour anions. In the PH$_4$I structure the cations are instead coordinated to eight anions, of which four are slightly closer to the cations than the other four. As the pressure increases, however, the anion–cation distances approach those of the B2 structure, in which the cation is in a symmetric 8-fold coordinated sites. The increase of coordination number as the pressure increases, suggests that the oxide becomes more ionic at higher pressures.

At zero temperature and pressure FeO is stable in the r-B1 structure, but transforms into a B8 or *i*-B8 structure at higher pressures [33,34]. It has also been suggested that the *i*-B8 and B8 polymorphs may co-exist [34,35]. Above the Néel temperature (198 K at ambient pressure [36]) FeO also has the B1 structure, and is iso-structural with the alkaline earth oxides. Experimentally the B1 structure is proposed to transform into a B8 polytype at ca. 96 GPa and 700 K [33], while the r-B1 to B8-type of transition has not yet been experimentally characterised.

One common feature of systems containing transition metal ions is the possibility to change from high-spin (HS) to low-spin (LS) states. For FeO it is, therefore, not only important to investigate the structural variations as a function of pressure, but also possible spin transitions that give rise to different magnetic structures. In this paper, we discuss the anti-ferromagnetic (AFM) and non-magnetic (NM) structures of FeO (see figure 1c). In the AFM B1 and r-B1 structures, the Fe^{2+} ions have a HS configuration with four un-paired electrons (Fe^{2+} is a d^6 ion), which give rise to a magnetic moment on the Fe^{2+} ions. In these structures the magnetic moments are aligned within the [1 1 1] plane [37], as indicated in figure 1c. It has also been proposed that the high-pressure polymorphs, *i*-B8 and B8, show AFM structures [35,38], in which the magnetic moments are aligned within the [1 1 0]-planes (see figure 1c). In a Mössbauer study by Pasternak *et al.* [39] it was proposed that the HS configuration of the Fe^{2+} ions undergoes a spin transition to a LS configuration at ca. 120 GPa. A low spin state results in a NM structure, since the Fe^{2+} ions in this situation have no un-paired electrons. On the other hand, in an XES study by Badro *et al.* [40] this HS to LS transition was not observed at pressures up to 140 GPa. Hence, one suitable application of the hybrid functionals is to investigate whether an HS to LS transition can occur in FeO as a function of pressure, and to understand if this transition is associated with metallisation.

2. Methods

All calculations were performed with the CRYSTAL 2003 code (CR03) [41]. In this program the crystalline orbitals are expressed as linear combinations of Bloch functions, which in turn are built up from Gaussian-type orbitals (GTO). In CR03, periodic self-consistent-field (SCF) calculations can be performed both within the HF scheme, as well as with various functional formulations within DFT. Not only is it possible to combine different exchange

and correlation functionals, it is also possible to mix the HF and DFT exchange functionals to any desired degree. We can, therefore, use different exchange ratios to investigate different observables, such as the electronic and geometric structures of the oxides. The latter approach provides us a computationally tractable way to study strongly correlated systems, including FeO [7,13].

In this paper, we mix the Hartree-Fock (F; also referred to as the Fock-exchange) with the Slater (S) [42], Becke (B) [5] or Perdew-Wang 91 (P) [43–46] exchange functionals, in combination with the Vosko-Wilk-Nusair (VWN) [47], LYP [6] or Perdew-Wang91 (PW91) [43–46] correlation functionals. The generic hybrid functional with a percentage α of Fock-exchange is indicated with the shorthand notation F$_\alpha$X$_{100-\alpha}$C, where X and C are the acronyms of the DFT exchange and correlation functionals employed, as indicated above. For example, F$_{35}$B$_{65}$LYP will represent:

$$F_{35}B_{65}LYP = 35X(F) + 65X(B) + C(LYP), \qquad (1)$$

α can be treated as an empirical parameter, allowing us to monitor how the calculated properties vary by tuning the α-value between 0 and 100%. This procedure allows us to select the α-value that best reproduces the experimental observables. All calculations for FeO are spin polarised.

The exchange-correlation potential was expanded numerically, and the cut-off threshold parameters (ITOLs) for the selection of the Coulomb and Exchange integrals were set to {8 8 8 8 16}. We used a k-point mesh of 10 × 10 × 10, expanded according to the Monkhorst-Pack scheme. The Broyden mixing, as implemented in CR03 [41], was employed for the metallic solutions, while for the insulating solutions we employed the level shifting technique [48] for faster convergence. In all calculations we used the same all-electron basis set for oxygen, i.e. 8-411Gd1 [49]. For the cations we used all-electron basis sets for Mg (8-611Gd1 [49]), Ca (86-511Gd3 [3]) and Fe (86-411d41 [50]), while for Sr and Ba we used Hay-Wadt's small core effective core potentials (ECP) in combination with the 31Gd3 [3] and 31Gd1 [3] Gaussian-type of valence basis sets for Ba and O, respectively. The GTOs employed in our study are optimised in the B1 structure, and we did not re-optimise the basis sets for the different polymorphs, as was instead done in Ref. [3]. We should, however, bear in mind that basis set effects may be important when determining phase transition pressures.

All structure optimisations are performed at constant pressure, employing the DOMIN-algorithm [51], which is a BFGS-method, to optimise the lattice parameters. To optimise the atomic positions we instead use the Berny-algorithm [52]. Both the DOMIN- and Berny-algorithms are implemented in the CR03 code.

For calculations at constant pressure we have optimised the enthalpy (*H*):

$$H = E + PV, \qquad (2)$$

of the system, where *E* is the internal energy, *V* the volume and *P* the pressure (not to be mistaken with the symbol *P* indicating the PW91 exchange functional).

The pressures associated with the various phase transitions were obtained using two different techniques. For CaO, BaO and FeO we fitted the calculated enthalpy values for each polymorph to a fifth-order polynomial of pressure. At the phase transition the enthalpy difference ($\Delta H_T(P)$) fulfils the condition:

$$\Delta H_T(P) = H_A(P) - H_B(P) = 0 \qquad (3)$$

where $H_A(P)$ and $H_B(P)$ denote the calculated enthalpies for the two polymorphs (A and B) at the given pressure.

For comparison with Ref. [3] we also calculated the transition pressure (P_T) between the B1 $\leftrightarrow$ B2 polymorphs of MgO, CaO and SrO starting from the Murnaghan equation of state [53], which yields the internal energy according to:

$$E_{Murn}(V) = -E_0 + \frac{B_0 V}{B'} \left\lfloor \frac{(V_0/V)^{B'}}{B' - 1} + 1 \right\rfloor - \frac{V_0 B_0}{B' - 1} \quad (4)$$

where E_0 and V_0 denote the equilibrium energy and volume, and B_0 and B' are the bulk modulus and its derivative, respectively. With the knowledge that

$$P = -\frac{\partial E}{\partial V} \qquad (5)$$

we can express the enthalpy as function of pressure according to:

$$H(P) = E_0 + \frac{V_0 B}{B' - 1} \left[\left(\frac{B'}{B} P + 1 \right)^{1 - \frac{1}{B'}} - 1 \right] \qquad (6)$$

The calculated bulk moduli are obtained by fitting the Murnaghan equation of state.

Scanning the phase diagram of one mineral is in general computationally very expensive, since it includes a range of calculations at different pressures for all the possible magnetic and structural polymorphs. For some compounds we are required to perform between 50 and 100 calculations per functional to determine the phase diagram solely as a function of pressure. In this project we have particularly taken advantage of the Condor-cluster, which is built and maintained at UCL [54,55]. In this cluster we have access to more than 900 MS-Windows based machine, and because our calculations are independent on each other, we can submit all jobs we need to determine the phase diagram of one compound at the same time. After analyses our data are stored at the SRB [56,57] vaults available within the eMinerals project [58]. Currently, these vaults are located at the Daresbury Laboratory, Cambridge University and UCL in London. This solution also makes it easy for other groups to access the stored data, and it facilitates collaborations between the different groups within the project.

3. Results on MgO, CaO and SrO

3.1 Effect of exchange and correlation functional on V_0 and B_0

In this section, we describe how the mixing of different amounts of Fock-exchange (α) in combination with the different exchange (B, P and S) and correlation (LYP, PW91 and VWN) DFT functionals influences the optimised bulk volumes and moduli. We discuss CaO in detail because it is the compound for which we have the most accurate experimental and theoretical data available.

Our first aim is to determine how the different *correlation functionals* (VWN, LYP and PW91) reproduce the experimentally reported volumes and bulk moduli in combination with the $F_\alpha B_{100-\alpha}$ hybrid exchange functionals. The optimised geometries (V_0) and bulk moduli (B_0) at zero pressure for CaO, obtained from Murnaghan's equation of state (equation 4), are reported in figure 2. For comparison we also calculated V_0 and B_0, without any correlation functional.

Independently on the correlation functional chosen, we see from figure 2a that all the equilibrium volumes become smaller as the amount of Fock-exchange (α) increases, but
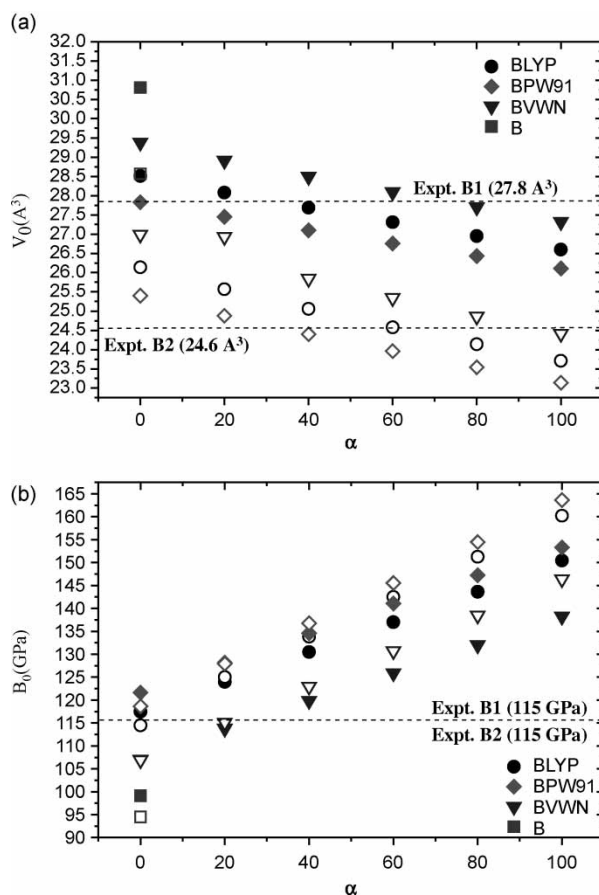

Figure 2. Optimised (a) volumes and (b) bulk moduli (at zero pressure) as a function of Fock-exchange (α) for CaO, using different correlation functionals combined with $F_{\alpha 100-\alpha}$ exchange functional. Closed and open shapes represent the B1 and B2 structures, respectively. Experimental values from Refs. [15, 16 and 26].

for the same value of α the PW91-correlation functional gives the smallest and the VWN-functional the largest volume. We also find that all three correlation functionals reduce V_0 compared to a functional with no correlation. These observations are the same for both the B1 and B2 structures; however, in figure 2a we see that, for each functional, the errors compared to the experimental values in the equilibrium volumes for the B1 and B2 structures are different. Furthermore, we find that the B2 structure in general requires more Fock-exchange than the B1 structure to correctly reproduce the experimentally reported V_0 values of 24.6 and 27.8 Å [15], respectively.

As shown in figure 2b, increasing the amount of Fock-exchange increases the value of the bulk moduli. As expected the larger values of V_0 give rise to a smaller B_0 in both the B1 and B2 structures, and consequently, the Becke exchange-functional without any correlation gives rise to smaller bulk moduli than the functionals containing electron correlation.

Let us now examine the effect of different formulations of the DFT *exchange functional* in the hybrid. In order to do this, we fix the correlation functional to its PW91 formulation, and vary the type of exchange functional in the hybrid. Results are plotted in figure 3. When comparing the two GGA functionals (*B* and *P*), we find very little difference in the V_0 and B_0 values for the B1 structure. Both curves show smaller V_0 and higher B_0 values as α increases.

However, using the LDA functionals (Slater exchange and VWN-correlation) in the hybrid functional ($F_\alpha S_{100-\alpha}$VWN) produces smaller volumes compared to the $F_\alpha B_{100-\alpha}$VWN functionals (see figure 3a). Interestingly, the volumes increase as the amount of Fock-exchange increases, which is the opposite behaviour to that observed with the GGA exchange functionals. As a consequence B_0 becomes smaller as α increases (figure 3b) for the $F_\alpha S_{100-\alpha}$VWN functionals, but larger for the $F_\alpha B_{100-\alpha}$-VWN functionals.

The B2 structures, in which cation and anion have higher coordination number, are expected to be more ionic than the B1 structure; as we have seen, the B2 structure needs a higher percentage of Fock-exchange to correctly reproduce the experimental V_0 values (see figure 2a). The explanation for the need of more Fock-exchange is due to the competition between the long-ranged electrostatic and the short-ranged covalent contributions; when increasing the amount of Fock-exchange we obtain a more localised solution which give rise to a higher Madelung-field, which is in better agreement with the true solution for the ionic compounds than the more delocalised (and thus covalent) solution obtained using pure DFT.

Since also the cation type modifies the ionicity of the solid, we include in our investigation how the cation type influences the V_0 and B_0 values. This can be achieved by comparing MgO, CaO and SrO. We expect the ionicity to decrease according to MgO > CaO > SrO because we find that the 3-d orbitals show important hybridisation with the neighbouring oxygen already for Ca. In this study,
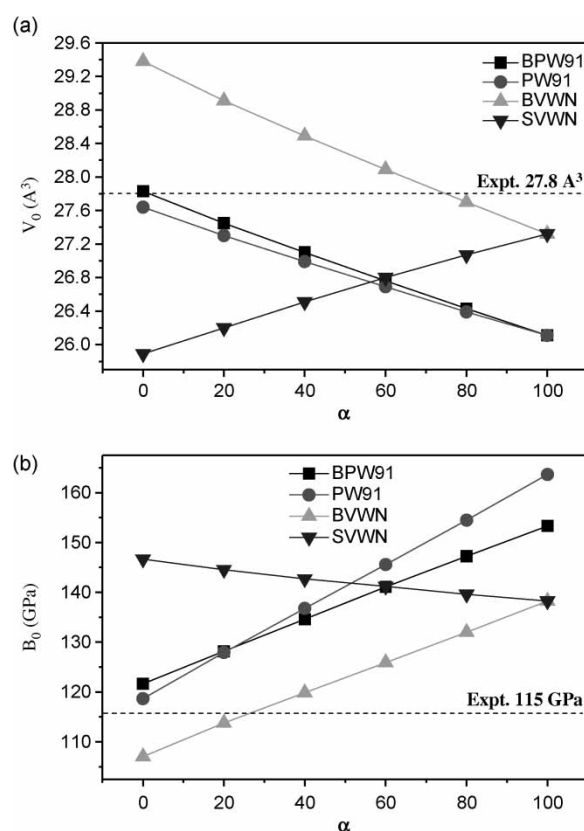

Figure 3. Optimised (a) volumes and (b) bulk moduli for B1 structure of CaO, using different combinations of exchange and correlation functionals. Experimental values from Refs. [16 and 26].

we only include the $F_\alpha B_{100-\alpha}$ LYP hybrid functionals. As demonstrated in figure 4a again the V_0 values decrease as the percentage of Fock-exchange increases. The same behaviour is observed for all three oxides, but the amount of Fock-exchange required for reproducing the experimental volumes decreases as the size of the cation increases: MgO needs ca. 40% and SrO 0% Fock-exchange to reproduce the experimental values of 18.5 Å [59] and 34.3 Å [17], i.e. again we find that the more ionic the structure, the more Fock-exchange is required to reproduce the experimental data. B_0 values are again following the trends in V_0 and are getting smaller as α increases (figure 4b).

3.1.2 B1 ↔ B2 phase transitions in MgO, CaO and SrO.

At this point we turn to investigate how the transition pressure (P_T) for the pressure-induced B1 ↔ B2 phase transition in the alkaline earth oxides is predicted by using the hybrid functionals. In figure 5 we present the value of P_T calculated employing three different $F_\alpha B_{100-\alpha}$ combinations in the $F_\alpha B_{100-\alpha}$LYP series, and the SVWN (LDA) functionals. As discussed in the "Introduction" section, the GGA-methods, including BLYP, often overestimate P_T in comparison to experiment. It is, therefore, not surprising to find that this is also the case in our calculations on CaO, where BLYP predicts a P_T value of ca. 84 GPa, compared with an experimental value of ca.
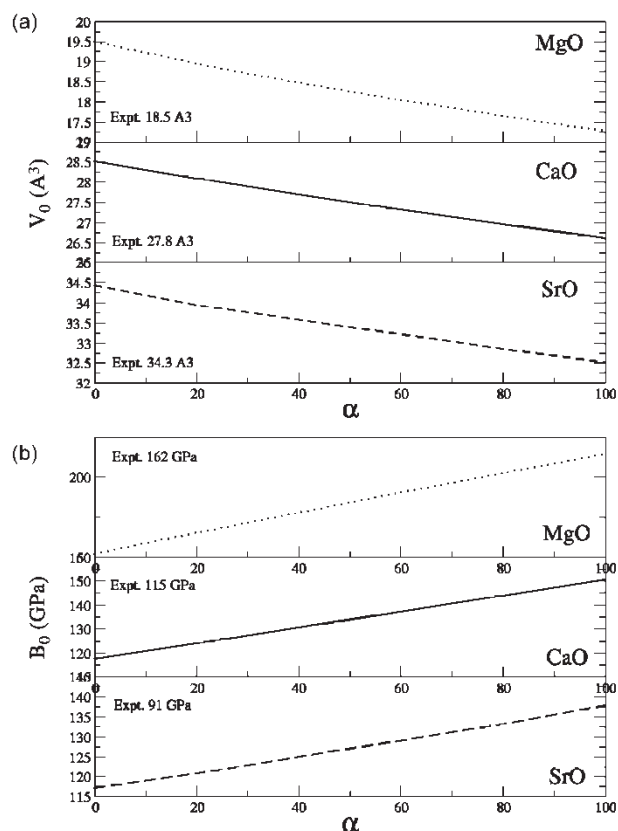
Figure 4. Optimised (a) volumes and (b) bulk moduli for the B1 structures of MgO, CaO and SrO, using the $F_{?\alpha}B_{100-\alpha}LYP$ functionals. Experimental values are taken from Refs. [16,17,51 and 56].

experimental value is obtained using the LDA functional (SVWN), i.e. the one that yields the worst agreement for the equilibrium volumes.

We also calculated P_T from Murnaghan's equation of state (see equation 6); these results are presented in Table 1. Firstly, we note that the two methods employed in our investigation (compare Table 1 and figure 5a–c) give good agreement with each other when the same exchange and correlation functionals are combined. We also find that, as the amount of Fock-exchange increases, P_T decreases. Only for the combinations between Fock- and Slater exchange ($F_\alpha S_{100-\alpha}VWN$) is it found that P_T increases as the amount of Fock-exchange increases, thus, following the same behaviour as previously discussed for V_0.

In figure 6 we show that P_T decreases in the order of MgO > CaO > SrO. Moreover, in figure 6 we observe that as α increases for CaO and SrO, P_T decreases. In contrast, MgO exhibits a different behaviour with a maximum in P_T for α around 60%. All calculated P_T values (450–550 GPa) are in good agreement with previous theoretical investigations, which found a range of values for P_T from 450 to 660 GPa (e.g. [3,18,21,28–30]).

4. $B1 \leftrightarrow B8 \leftrightarrow PH_4I \leftrightarrow B2$ Phase Transitions in BaO

Most theoretical investigations on the phase transitions in BaO have focused on the $B1 \leftrightarrow B2$ transition, while only two theoretical studies have investigated the full experimentally proposed sequence $B1 \leftrightarrow i-B8 \leftrightarrow PH_4I \leftrightarrow B2$. One used plane-wave calculations [60], and the second a sophisticated inter-atomic potential model (AIM) [61]. Experimentally Weir *et al.* [31] and Liu *et al.* [32] proposed that the B1 structure at room temperature undergoes a phase transition to an *i*-B8 structure at ca.

60 GPa [15,26]. Increasing the amount of Fock-exchange in the hybrid slightly reduces the calculated pressure of the phase transition, bringing it closer to the experimental value. Nevertheless, the best agreement with the
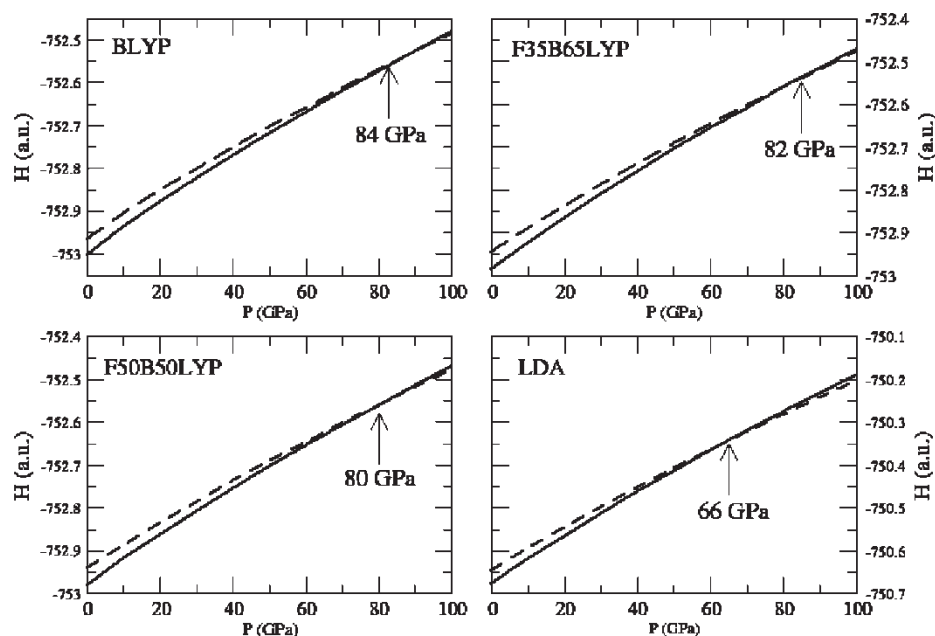

Figure 5. Transition pressures (P_T) for CaO using the (a) BLYP; (b) $F_{35}B_{65}LYP$; (c) $F_{50?}B_{50}LYP$; and (d) SVWN functionals. P_T calculated from equation 3.

Table 1. Transition pressures (P_T) for B1 $\leftrightarrow$ B2 transition in CaO, using different functionals.

α	$F_\alpha B_{100-\alpha}LYP$	$F_\alpha B_{100-\alpha}PW91$	$F_\alpha B_{100-\alpha}VWN$	$F_\alpha P_{100-\alpha}PW91$	$F_\alpha S_{100-\alpha}VWN$
0	84	73	87	73	65
20	82	71	88	71	69
40	80	70	86	70	74
60	78	68	84	68	75
80	76	67	81	67	76
100	72	65	78	65	78
Expt. [15]	60				

P_T is calculated from equation 6. Pressures are given in GPa, and α denotes the amount of Fock-exchange in percentage.

10 GPa, and then transforms into a PH$_4$I type of structure at ca. 15 GPa. The latter structure can be regarded as a distorted B2 structure, and indeed as the pressure increases the extent of the distortion decreases and the PH$_4$I structure strives towards the B2.

In this study, we employ different Hamiltonians, namely BLYP, $F_{35}B_{65}LYP$, $F_{50}B_{50}LYP$ and LDA, to study the full sequence of phase transitions proposed experimentally. Optimising the enthalpies as a function of pressure we determine the phase transition by fitting the function ΔH_T to a fifth order polynomial (equation 3). As for CaO, we here find that that as the amount of Fock-exchange increases the pressure of the predicted phase transitions decrease (see Table 2).

We start with the B1 to i-B8 phase transition, which is experimentally observed at ca. 10 GPa. Uludogan *et al.* [60] performed plane-wave calculations with the PW91 functional, and reported the phase transition to occur at ca 11 GPa, while our P_T value using the BLYP functional is 20 GPa. Considering the P_T values for CaO reported in Table 1, we notice that the phase transition pressure calculated with the PW91 functional is lower than that predicted with the BLYP; comparison between the B1 to i-B8 transition pressure calculated here with the results of Ref. [60] is consistent with this trend. However, since GGA functionals usually overestimate the P_T-values we suggest that the excellent agreement between Ref. [60] and the experimental value by Weir *et al.* [31] could also
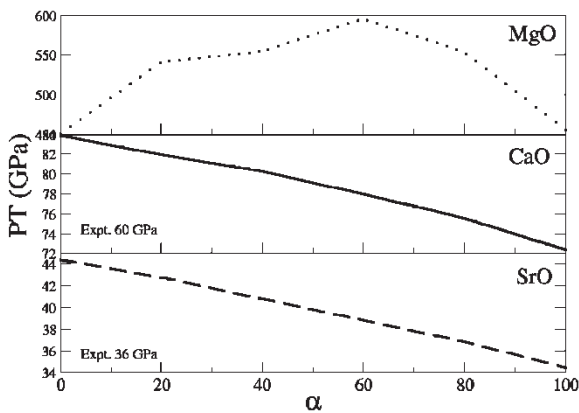

Figure 6. Transition pressures (P_T) for the B1 $\leftrightarrow$ B2 transition in MgO, CaO and SrO. The experimental value of CaO and SrO are 60 GPa [15,26] and 36 GPa [17], respectively. All calculations are performed with the $F_\alpha H_{1-\alpha}LYP$ functionals.

be associated with the choice of pseudo-potentials used in Ref. [60]. Our $F_{50}B_{50}LYP$ functional predicts this phase transitions to occur at ca. 18 GPa, while the LDA Hamiltonian predicts a P_T value of 5 GPa. In Ref. [56] the pressure of the phase transition was estimated as ca. 12 GPa using the AIM model.

For the i-B8 $\leftrightarrow$ PH$_4$I transition the hybrid functionals yield similar P_T values as the BLYP functional ($P_T \sim$ 27 GPa), while the LDA Hamiltonians predicts a phase transition at ca. 13 GPa. The experimental value given in Ref. [31] is about 15 GPa, while the calculated values in Refs. [60] and [61] are of 22 and 19 GPa, respectively. Again the P_T value obtained with the PW91 functional [60] is lower than the P_T value calculated at the BLYP level.

The last BaO phase suggested to exist in the experimental study is the high-symmetry B2. This has not been directly observed, but the distorted PH$_4$I gradually evolves towards the B2 structure on increasing pressure. The PH$_4$I $\leftrightarrow$ B2 phase transition can therefore take place in two ways: either via an abrupt (first-order) phase transition, or via a gradual (second-order) evolution of the PH$_4$I structure towards the higher symmetry B2 phase. A computational study can help us answering this question: in the former case the calculated enthalpy of the two phases will cross as a function of pressure; in the latter, the calculated enthalpy of the PH$_4$I phase will tend asymptotically to that of the B2 structure, without crossing it. Experimental evidence [31] shows that, in the range of pressure examined, the PH$_4$I structure constantly approaches the B2 structure, and the latter was not actually observed since the experiments only reached pressures of 60 GPa. Our calculations, with each of the four functionals employed, predict the existence of a first-order PH$_4$I $\leftrightarrow$ B2 phase transition. The transition pressure is calculated as ca. 62 GPa at the BLYP level, while the hybrid functionals anticipate the phase transition at 44–48 GPa. The calculated P_T value for the LDA functional is 50 GPa. In the paper by Uludogan *et al.* [60] the PH$_4$I $\leftrightarrow$ B2 P_T was predicted at ca. 62 GPa. On the other hand, the AIM study by Aguado *et al.* [61] predicted the same transition to occur at only 25 GPa, employing lattice static calculations. The reasons the latter authors calculate a lower P_T is discussed in Ref. [61], one explanation is that the AIM potential is not accurate enough to differentiate between the small energy differences associated with the different polymorphs. Nevertheless, all the computational studies agree in predicting the existence of a PH$_4$I $\leftrightarrow$ B2 transition.

Table 2. Pressure transitions (P_T) for the B1 ↔ *i*-B8 ↔ PH-$_4$I ↔ B2 phase transitions in BaO calculated for different Hamiltonians using equation 3.

	P_T *(GPa)*		
Hamiltonian	*B1 → i-B8*	*i-B8 → PH₄I*	*PH₄I → B2*
BLYP	20	26	62
F$_{35}$B$_{65}$LYP	19	27	49
F$_{50}$B$_{50}$LYP	18	27	44
LDA	5	13	50
PW91 [55]	11	22	62
AIM [56]	12	19	25
Expt. [31]	10	15	>60

Comparisons are made to the experiment and other theoretical studies.

This observation, however, does not rule out the possibility of a gradual evolution of the PH$_4$I into the B2 phase. Again, calculations provide a suitable tool to investigate this topic. The distortion leading from the PH$_4$I to B2 structure is characterised by two structural parameters: firstly the c/a ratio, which equals $1/\sqrt{2}$ (∼0.705) in the B2 phase while is higher in the distorted PH$_4$I, and secondly the fractional coordinate of the cation, which is (1/2,0,1/2) in the B2 and (1/2,0,1/2 + Δ) in the PH$_4$I structure. We have studied the evolution of both c/a ratio and of the parameter Δ as a function of pressure.

The c/a ratio is known also from the experimental work, and Weir *et al.* [31] showed that the c/a-ratio slowly approaches the $1/\sqrt{2}$-value (∼0.705), which is characteristic for the B2 structure, on increasing pressure. In figure 7 we demonstrate that the BLYP, as well as the hybrid functionals, predict a decreasing value of c/a as function of pressure, in agreement with experiment, but in none of the functionals the c/a ratio has yet reached the $1/\sqrt{2}$ value at 70 GPa, which is the highest pressure we considered. Our results are in excellent agreement with the AIM-values obtained by Aguado *et al.* [61], using molecular dynamics simulations (at room temperature) even though all theoretical values are underestimated compared to the experimental ones. This observation may be related to kinetic effects, which change the energy barriers for the atomic displacements. However, we want to emphasise that it can be either the MD
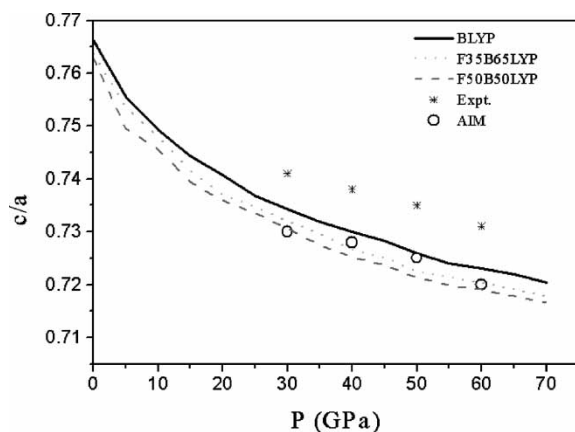
simulations; the experimental work or both which are underestimating the entropy effects since both investigations are done at relatively low temperatures.

Investigating the lattice parameters (*a*- and *c*-axes) separately we find that the *c*-axis shows the largest compressibility, changing from 3.6 to 3.05 Å, corresponding to ca. 15%, while the *a*-axis shows a change of ca. 7.5% (see figure 8). At zero pressure we find that both the *a*- and *c*-axes are overestimated compared to the experimental values, but as the pressure increases we find good agreement between calculated and experimental ones. At 14 GPa the lattice parameters are 4.375 and 3.25 Å [31] for the *a*- and *c*-axes, respectively.

Let us now examine the change that occurs in the parameter Δ, representing the displacement of the Ba ion in the PH$_4$I phase, as a function of pressure. The parameter Δ is zero in the B2 structure (see figure 9). At 70 GPa we find that the Δ-values are between 0.07 and 0.08 for the different functionals, while at zero pressure they are roughly 0.17 fractional units. Experimentally the Δ-value is 0.06 at 60 GPa [20]. As for the c/a-ratio (see figure 7), using the F$_{50}$B$_{50}$LYP functional the parameter Δ approaches its value in the B2 phase more rapidly than with the BLYP and the F$_{35}$B$_{65}$LYP functionals, suggesting that the phase transition should be observed at lower P_T when the amount of Fock-exchange increases, which is in line with the behaviour observed for the other phase transitions.

5. *i-B8(AFM)* ↔ *B8(NM)* Phase Transition in FeO

In Table 3 we report pressure transitions between the high-pressure structures of B8-type in FeO, considering the four different FeO polymorphs: *i*-B8(AFM); *i*-B8(NM); B8(AFM); and B8(NM). We have in this case employed six different functionals. The aims of the current study on FeO are to: (i) determine a possible HS to LS transition on the Fe^{2+} ions; and (ii) establish if the high-pressure structures are metallic.

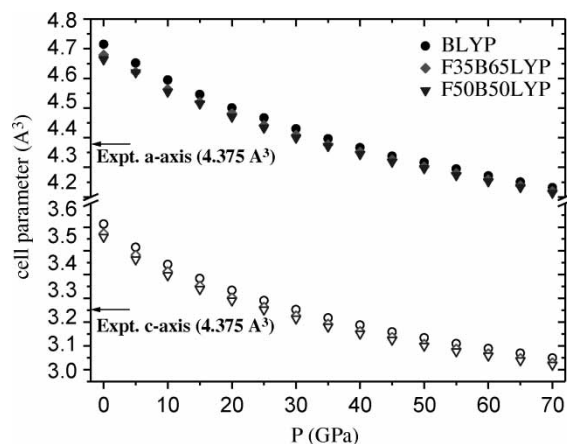Figure 7. c/a ratio for the PH$_4$I structure of BaO as a function of pressure.

Figure 8. Optimised *a*- and *c*-axes as function of pressure for the PH$_4$I structure of BaO. Closed and open shapes represent *a*- and *c*-axes, respectively. Experimental values from Ref. [31].
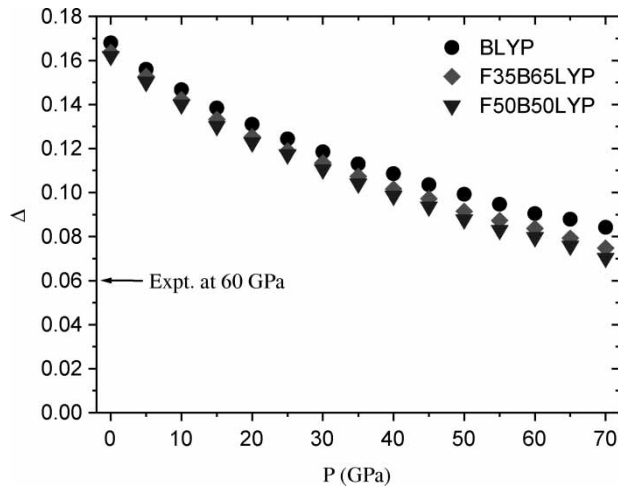
Figure 9. Δ-value as function of pressure for the PH$_4$I structure of BaO. Experimental value from Ref. [31].

From our calculations we find that the enthalpy differences between the *i*-B8(AFM) and B8(AFM), as well as the B8(NM) polymorphs are indeed small, but for each functional, the *i*-B8(AFM) polymorph is predicted to be energetically the most stable one at pressures higher than 90 GPa. This finding is in agreement with previous theoretical investigations [35,38]. Yet the enthalpy differences are small, and we can, therefore, not rule out the possibility of co-existing polymorphs discussed in Refs. [34] and [35]. Consequently, the phase transitions listed in Table 3 could be expected to occur over a broad pressure range. We also show that the pressure-induced phase transition predicted using the different functionals is the same, namely an *i*-B8(AFM) ↔ B8(NM) transition at $P > 90$ GPa, which means that the structural phase change is associated with a magnetic phase transition, involving a HS to LS transition on the Fe^{2+} ions. Hence, our calculations predict a spin breakdown in the range of 145–190 GPa, depending on the functional. We would like to emphasise that the pressures associated with the *i*-B8(AFM) to B8(NM) transitions from our CR03 calculations are lower than the pressure reported by Cohen *et al.* [63] using a GGA functional. The latter authors reported a spin break down at ca. 200 GPa calculated in for B1 structure, using the Stoner model. One fundamental difference between our calculations and those reported in Ref. [63] are that we report a spin-break

down associated with a structural phase transitions, while in Ref. [63] the spin break down is associated with one and the same structure, the B1 structure, which in fact is the low-pressure structure.

As for the previous oxides discussed in this paper we find that the gradient-corrected functionals (BLYP and PW91) result in higher P_T than the LDA (SVWN) functional. This is also the case for FeO (see Fig. 11), but while for CaO, SrO and BaO we found that as the amount of Fock-exchange increases P_T decreases, the case for FeO is different, as can bee seen from Figs. 11e and f. F$_{50}$B$_{50}$LYP exhibits a higher P_T than F$_{35}$B$_{65}$LYP. FeO shows therefore a similar behaviour to MgO, with a maximum in P_T as α increases (see figure 6). Bearing in mind that the LS configuration of the Fe^{2+} ion has a similar ionic size and properties as the Mg^{2+} ion, this behaviour is not entirely surprising, but we also believe that the similarity of MgO and FeO needs to be studied in more detail elsewhere.

The density-of-states (DOS) from all functionals investigated show that the *i*-B8(AFM) structure is insulating, while the B8(NM) is metallic (see figure 10). Hence, the *i*-B8(AFM) ↔ B8(NM) is also coupled with an insulator to metal transition. The origin of the metallisation is due to an important overlap between the Fe*3d* and O*2sp* crystal orbitals, which is associated with the higher symmetry of the B8(NM) than the *i*-B8(AFM) structure.
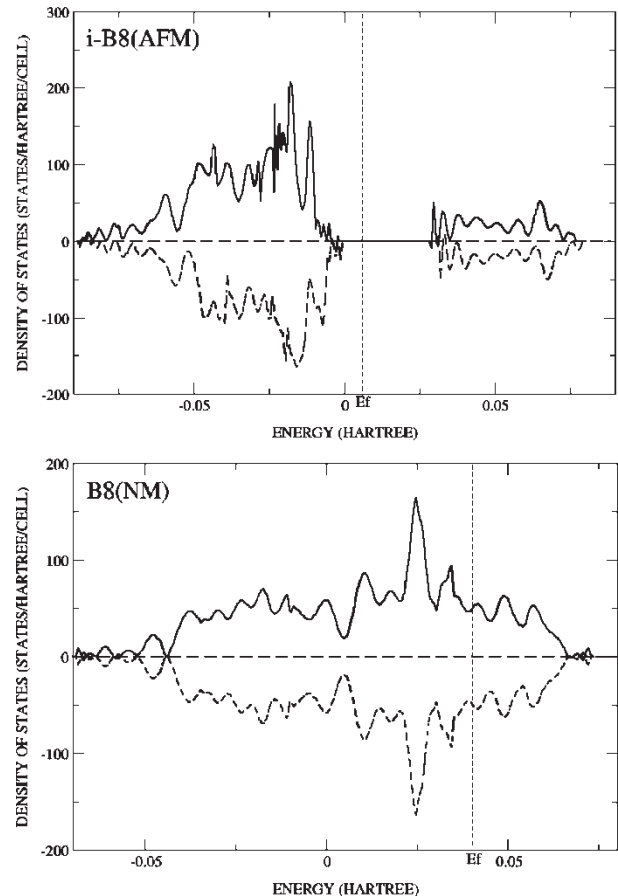

Table 3. Pressure transitions (P$_T$) in FeO calculated for different Hamiltonians using equation 3.

Hamiltonian	P_T (GPa)	
	B8(AFM) → *i*-B8(AFM)	*i*-B8(AFM) → B8(NM)
BLYP		181
F$_{35}$B$_{65}$LYP	68	145
F$_{50}$B$_{50}$LYP	85	155
B3LYP	25	192
PW91 [55]		213
LDA		150

Figure 10. Total density-of-states (DOS) for the (a) *i*-B8(AFM); and (b) B8(NM) structures at 140 GPa, using the H$_{35}$B$_{65}$LYP functional.

Experimentally the high-pressure polymorph of FeO is reported as being metallic [63].

6. Summary and conclusions

Below we summarise our findings, concerning the performance of hybrid functionals:

- By empirically fitting the amount of Fock-exchange in combination with different exchange and correlation functionals, we can reproduce the structural and elastic properties of all the oxides studied here. The issue was discussed in detail by Corà *et al.* [13], who concluded that the more ionic a compound the more Fock-exchange is required to reproduce the experimentally observed structural parameters, while to correctly reproduce the bulk moduli only between 20 and 30% Fock-exchange is required. Similar results were reported by Alfredsson *et al.* [7], and by Bredow *et al.* [10]. This is consistent with the fact that the B2 structure requires more Fock-exchange than the B1 structure. It also explains why the smaller and more ionic cations (Mg^{2+} and Ca^{2+}) require more Fock-exchange than the larger but less ionic Sr^{2+} cation.
- The hybrid functionals reproduce values of the transition pressures in between the P_T values obtained using the GGA and LDA Hamiltonians, following the trends observed for the equilibrium volumes. However, the P_T values are more difficult to reproduce than V_0 and B_0, since they depend on small energy and enthalpy differences.
- In contrast to structural and elastic properties, for which we found that the hybrid functionals containing Slater-exchange are in poor agreement with experiment, the $F_\alpha S_{100-\alpha}VWN$ hybrid functional is an attractive alternative to determine the transition pressure of oxides including heavy cations, such as SrO.
- We have also shown that the hybrid functionals correctly reproduce both insulators as well as metals, which imply that hybrid functionals can be successfully used to study insulator $\leftrightarrow$ metal transitions, such as the i-B8(AFM) $\leftrightarrow$ B8(NM) transition in FeO. This structural phase transition is associated with a magnetic phase transition. Hybrid functionals are able to reproduce the subtle changes in the structure associated with spin transitions.
- Using the Condor-cluster available at UCL in London, the real time required to study phase transitions is reduced from years to months. All data are effectively stored in the SRB vaults available in the E-minerals project.

Acknowledgements

References

[1] R.M. Martin. *Electronic structure—basic theory and practical methods*, Cambridge University press, Cambridge, UK (2004), and ref. there in.

[2] A. Zupan, M. Causa. Density-Functional LCAO Calculations for solids - Comparison among Hartree-Fock, DFT local-density approximation, and DFT generalised gradient approximation structural-properties. *Int. J. Quantum Chem.*, **56**, 337 (1995).

[3] M.-P. Habas, R. Dovesi, A. Lichanot. The B1 reversible arrow B2 phase transition in alkaline-earth oxides: a comparison of ab inition Hartree-Fock and density functional calculations. *J. Phys.: Condens. Matter*, **10**, 6897 (1998).

[4] N. Moll, M. Bockstedt, M. Fuchs, E. Pehlke, M. Scheffler. Application of generalised gradient approximations: The diamond - beta-tin phase transition of Si and Ge. *Phys. Rev. B*, **52**, 2550 (1995).

[5] A.D. Becke. Density-functional themochemistry. III The role of exact exchange. *J. Chem. Phys.*, **98**, 5648 (1988).

[6] C. Lee, W. Yang, R.G. Parr. Development of the Colle-Salvetti correlation-energy formula into a functional of the electron density. *Phys. Rev. B*, **37**, 785 (1988).

[7] M. Alfredsson, G.D. Price, C.R.A. Catlow, R. Orlando, S.C. Parker, J.P. Brodholt. Electronic structure of the antiferromagnetic B1-structures FeO. *Phys. Rev. B*, (2004) in press.

[8] F. Illias, R.L. Martin. Magnetic coupling in ionic solids studied by density functional theory. *J. Chem. Phys.*, **108**, 2519 (1998).

[9] I.de P.R. Moreira, F. Illas, R.L. Martin. Effect of Fock exchange on the electronic structure and magnetic coupling in NiO. *Phys. Rev. B*, **65**, 155102 (2002).

[10] T. Bredow, A.R. Gerson. Effect of exchange and correlation on bulk properties of MgO, NiO and CoO. *Phys. Rev. B*, **61**, 5194 (2000).

[11] W.C. Mackrodt, D.S. Middlemiss, T.G. Owens. Hybrid density functional theory study on vanadium monoxide. *Phys. Rev. B*, **69**, 115119 (2004).

[12] F. Corà. The performance of hybrid density-functional theory in solid state chemistry – the case of BaTiO3. *Mol. Phys.*, (2004) in press.

[13] F. Corà, M. Alfredsson, G. Mallia, D.S. Middlemiss, W.C. Mackrodt, R. Dovesi, R. Orlando. The performance of hybrid density functionals in solid state chemistry. In *Density Functional Theory in Inorganic Chemistry, Structure and Bonding*, J. McGrady, N. Kaltsoyannis (Eds), Vol. 20, Springer-Verlag, Heidelberg, 113, 117-232 (2004).

[14] N. Wilson, J. Muscat. The calculation of structural, elastic and phase stability properties of mineals using first principles techniques: A comparison of HF, DFT and hybrid functional treatments of exchange and correlation. *Mol. Sim.*, **28**, 903 (2002).

[15] P. Richet, H.K. Mao, P. Bell. Static Compression and equation of state of CaO to 1.35 Mbar. *J. Geophys. Res. (Solid Earth)*, **93**(15), 279 (1986).

[16] Y. Sato, R. Jeanloz. Phase Transition in SrO. *J. Geophys. Res.*, **86**, 1773 (1981).

[17] J.F. Mammone, H.K. Mao, P.M. Bell. Equation of State of CaO under static pressure conditions. *Geophys. Res. Lett.*, **8**, 140 (1981).

[18] A.R. Oganov, M.J. Gillan, G.D. Price. Ab initio lattice dynamics and structural stability of MgO. *J. Chem. Phys.*, **118**, 10174 (2003).

[19] M.J. Mehl, R.E. Cohen, H. Krakauer. Linearized augmented plane-wave electronic-structure calculations for MgO and CaO. *J. Geophys. Res. (Solid Earth)*, **93**, 8009 (1988).

[20] M.J. Mehl, R. Hemley, L.L. Boyer. Potential-induced breathing model for elastic moduli and high-pressure behaviour of the cubic alkaline-earth oxides. *Phys. Rev. B*, **33**, 8685 (1986).

[21] P. Cortona, A.V. Monteleone. Ab initio calculations of cohesive and structural properties of the alkali-earth oxides. *J. Phys.: Condens. Matter*, **8**, 8983 (1996).

[22] C.E. Sims, G.D. Barrera, N.L. Allan, W.C. Mackrodt. Thermodynamics and mechanism of the B1-B2 phase transition in group-I halides and group-II oxides *Phys. Rev. B*, **57**, 11164 (1998).

[23] S.I. Karato. *The dynamic structure of the deep Earth*, Princeton University Press, Princeton, US (2003).

[24] F.A. Cotton, G. Wilkinson. *Advanced Inorganic Chemistry; A Comprehensive Text*, 4th Ed., John-Wiley and Sons, New York (1980).

[25] The National Lime Association; www.lime.org.

[26] R. Jeanloz, T.J. Ahrens, H.K. Mao, P.M. Bell. B1-B2 transition in calcium-oxide from shock-wave and diamond-cell experiments. *Science*, **206**, 829 (1979).

[27] T.S. Duffy, R.J. Hemley, H.K. Mao. Equation of state and shear strength at Multimegabar Pressures: Magnesium Oxide to 227 GPa. *Phys. Rev. Lett.*, **74**, 1371 (1995).

[28] A.R. Oganov, P.I. Dorogokupets. All-electron and pseudopotential study of MgO: Equation of state, anharmonicity, and stability. *Phys. Rev. B*, **67**, 224110 (2003).

[29] N.D. Drummond, G.J. Ackland. Ab initio quasiharmonic equation of state for dynamically stabilized soft-mode materials. *Phys. Rev. B*, **65**, 184104 (2002).

[30] B.B. Karki, L. Stixrude, S.J. Clark, M.C. Warren, G.J. Ackland, J. Crain. Structure and elasticity of MgO at high-presure. *Am. Mineral.*, **82**, 51 (1997).

[31] S.T. Weir, Y.K. Vohra, A.L. Ruoff. High-pressure phase transitions and the equation of states of BaS and BaO. *Phys. Rev B*, **33**, 4221 (1986).

[32] L. Liu, W.A. Bassett. Effect of pressure on crystal-structure and lattice-parameters of BaO. *J. Geophys. Res.*, **77**, 4934 (1972).

[33] Y. Fei, H.K. Mao. In-situ determination of the NiAs phase of FeO at high-pressure and temperature. *Sicence*, **266**, 1678 (1994).

[34] M. Murakami, K. Hirose, S. Ono, F. Tsuchiya, M. Isshiki, T. Watanuki. High pressure and high temperature phase transition of FeO. *Phys. Earth and Plant. Inter.*, (2004) Article in press.

[35] I.I. Mazin, Y. Fei, R. Downs, R. Cohen. Possible polytypism in FeO at high pressures. *Am. Miner.*, **83**, 451 (1998).

[36] H. Bizette. Sur lorientation par le champ magnetique de quelques molecules et de quelques cristaux. *Ann. Phys.*, **1**, 295 (1946).

[37] N.C. Tombs, H.P. Rooksby. *Nature*, **165**, 442 (1950).

[38] Z. Fang, I.V. Solovyev, H. Sawada, K. Terakura. First-principles study on electronic structures and phase stability of MnO and FeO under high pressure. *Phys. Rev. B*, **59**, 762 (1999).

[39] M.P. Pasternak, R.D. Taylor, R. Jeanloz, X. Li, J.H. Nguyen, C.A. McCammon. High pressure collapse of magnetism in Fe0.94O: Mössbauer Spectroscopy beyond 100 GPa. *Phys. Rev. Lett.*, **79**, 5046 (1997).

[40] J. Badro, V.V. Struzhkin, J. Shu, R.J. Hemley, H.K. Mao. Magnetism in FeO at Megabar pressures from X-ray emission Spectroscopy. *Phys. Rev. Lett.*, **83**, 4101 (1999).

[41] V.R. Saunders, R. Dovesi, C. Roetti, R. Orlando, C.M. Zicovich-Wilson, N.M. Harrison, K. Doll, B. Civalleri, I.J. Bush. *CRYSTAL03, Users Manual*, University of Turin, Turin, Italy (2003).

[42] P.A.M. Dirac. *Proc. Cambridge Phil. Soc.*, **26**, 376 (1930).

[43] J.P. Perdew, Y. Wang. Accurate and simple density functional for the electronic exchange energy: Generalized gradient approximation. *Phys. Rev. B*, **33**, 8800 (1986).

[44] J.P. Perdew, Y. Wang. Erratum: Accurate and simple density functional for the electronic exchange energy: Generalise gradient approximation. *Phys. Rev. B*, **40**, 3399 (1989).

[45] J.P. Perdew, Y. Wang. Accurate and simple analytic representation of the electron-gas correlation energy. *Phys. Rev. B*, **45**, 13244 (1992).

[46] J.P. Perdew. *Electronic structure of Solids 1991*, Akademie Verlag, Berlin (1991).

[47] S.H. Vosko, L. Wilk, M. Nusair. Accurate spin-dependent electron liquid correlation energies for local spin-density calculations −a critical analysis. *Can. J. Phys.*, **58**, 1200 (1980).

[48] M.F. Guest, V.R. Saunders. Methods for converging open-shell Hartree-Fock wave-functions. *Mol. Phys.*, **28**, 819 (1974).

[49] M.I. McCarthy, N.M. Harrison. Ab initio determination of the bulk properties of MgO. *Phys. Rev. B*, **49**, 8574 (1994).

[50] Towler (1992), www.chimifm.unito.it/teorica/crystal/Basis_Sets/iron.html

[51] P. Spellucci. An SQP method for general nonlinear program using only equatlity constrained subproblems. *Math. Prog.*, **82**, 413 (1998) www.mathematik.tu-darmstadt.de/ags/ag8/Mitglieder/-spellucci_de.html.

[52] H.B. Schlegel. Optimization of equilibrium geometries and transition structures. *J. Comp. Chem.*, **3**, 214 (1982).

[53] F.D. Murnaghan. *Proc. Natl. Acad. Sci. USA*, **30**, 244 (1944).

[54] Paul Wilson, Wolfgang Emmerich, John Brodholt. Leveraging HTC for UK eScience with Very Large Condor pools: Demand for transforming untapped power into results. *Proceedings of the UK e-Science All Hands Meeting 2004*, 308−315 (2004), ISBN 1-904425-21-6.

[55] M. Calleja, R. Bruin, M.G. Tucker, M.T. Dove, R.P. Tyer, L.J. Blanshard, K. Kleese van Dam, R.J. Allan, C. Chapman, W. Emmerich, P.B. Wilson, J.P. Brodholt, A. Thandavan, V.N. Alexandrov. Collabrative grid infrastructure for molecular simulations: the Minerals, minigrid as a prototype integrated compute and data-grid. *Molecular Simulations*, pp. 317−328.

[56] R.W. Moore, C. Baru, Chapter 11. In *Grid Computing: Making The Global Infrastructure a Reality*, F. Berman, A.J.G. Hey, G. Fox (Eds), John Wiley, New York (2003).

[57] M. Doherty, K. Kleese, M. Williams, B. Strong, L. Blanshard, R. Tyer, T. Folkes, D. Corney, A. Sansum, M. Bly, N. White. *Proceedings of UK e-Science All Hands Meeting*, 51−58 (2003), (EPSRC, ISBN 1-904425-11-9).

[58] M.T. Dove, M. Calleja, J. Wakelin, K. Trachenko, G. Ferlat, P. Murray-Rust, N.H. de Leeuw, Z. Du, G.D. Price, P.B. Wilson, J.P. Brodholt, M. Alfredsson, A. Marmier, R.P. Tyer, L.J. Blanshard, R.J. Allan, K. Kleese van Dam, I.T. Todorov, W. Smith, V.N. Alexandrov, G.J. Lewis, A. Thandavan, S.M. Hasan. *Proceedings of UK e-Science All Hands Meeting 2003*, 302−305, (EPSRC, ISBN 1-904425-11-9).

[59] R.W.G. Wyckoff. *Crystal Structures*, 2nd Ed., Vol. 1, John Wiley and Sons, Inc, New York (1965).

[60] M. Uludogan, T. Cagin, A. Strachan, W.A. Goddard III. Ab initio studies of pressure induced phase transition in BaO. *J. Compt.-Aided Mat. Design*, **8**, 193 (2001).

[61] A. Aguado, L. Bernasconi, P.A. Madden. Interionic potentials from ab initio molecular dynamics: The alkaline earth oxides CaO, SrO and BaO. *J. Chem. Phys.*, **118**, 5704 (2003).

[62] R.E. Cohen, I.I. Mazin, D.G. Isaak. Magnetic collapse in transtition metals oxides at high pressures: Implication for the Earth. *Science*, **275**, 654 (1997).

[63] E. Knittle, R. Jeanloz. High-pressure metallization of FeO and implications for the Earth Core. *Geophys. Res. Lett.*, **13**, 1541 (1986).

[64] O.L. Anderson, P. Andreatch Jr.. *J. Am. Ceram. Soc.*, **49**, 404 (1966).